Published by Institute of Physics Publishing for SISSA/ISAS
Received: *August 9, 2002*
Accepted: *November 18, 2002*

Study of the Higgs-boson decays into W^+W^- and ZZ at the Photon Collider

Piotr Nieżurawski and Aleksander Filip Żarnecki

Institute of Experimental Physics, Warsaw University
ul. Hoza 69, 00-681 Warsaw, Poland
E-mail: Piotr.Niezurawski@fuw.edu.pl, Filip.Zarnecki@fuw.edu.pl

Maria Krawczyk

Institute of Theoretical Physics, Warsaw University
ul. Hoza 69, 00-681 Warsaw, Poland, and
Theory Division, CERN
CH-1211 Geneva 23, Switzerland
E-mail: Maria.Krawczyk@fuw.edu.pl

Abstract: Production of the Standard Model Higgs-boson at the photon collider at TESLA is studied for Higgs-boson masses above 150 GeV. A simulation of signal and background processes takes into account realistic luminosity spectra and detector effects. In the considered mass range, large interference effects are expected in the W^+W^- decay channel. By reconstructing W^+W^- and ZZ final states, not only the $h \to \gamma\gamma$ partial width can be measured, but also the phase of the scattering amplitude. This opens a new window onto the precise determination of the Higgs-boson couplings. Models with heavy, fourth-generation fermions and with enlarged Higgs sector (2HDM (II)) are considered.

Keywords: Standard Model, Beyond Standard Model, Higgs Physics.

© SISSA/ISAS 2002

http://jhep.sissa.it/archive/papers/jhep112002034/jhep112002034.pdf

JHEP11(2002)034

Contents

1. Introduction **1**

2. Vector boson production **2**

3. Analysis **7**

3.1 Luminosity spectra 7

3.2 Simulation 8

3.3 Event selection 8

3.3.1 W^+W^- events 9

3.3.2 ZZ events 11

3.4 Mass resolution 11

3.5 Parametrization 12

4. Results **13**

5. Summary **14**

1. Introduction

A photon collider has been proposed as a natural extension of the e^+e^- linear collider project TESLA [1]. The physics potential of a photon collider is very rich and complementary to the physics program of e^+e^- and hadron colliders. It is the ideal place to study the mechanizm of the electroweak symmetry breaking (EWSB) and properties of the Higgs boson. If the Standard Model Higgs-boson mass is below $\sim 140\,\mathrm{GeV}$, its properties can be measured in detail using the $h \to b\bar{b}$ decay channel. However, if its mass exceeds 170 GeV the $b\bar{b}$ branching ratio goes below 1% and we have to consider other decay channels for a precise measurement of the Higgs-boson. In this paper the feasibility of measuring Higgs-boson production using the W^+W^- and ZZ decay channels will be considered. Because of the interference with other Standard Model contributions, the process turns out to be sensitive not only to the Higgs-boson partial width to $\gamma\gamma$, $\Gamma_{\gamma\gamma}$, but also to the phase of the $\gamma\gamma \to h$ amplitude, $\phi_{\gamma\gamma}$. A precise measurement of both $\Gamma_{\gamma\gamma}$ and $\phi_{\gamma\gamma}$ is important for a unique determination of the Higgs-boson couplings and can turn out to be crucial in distinguishing between different models of "new physics", see also [2]–[5].

Prospects for measuring Higgs-boson production at the Photon Collider in the W^+W^- and ZZ decay channels has been previously considered in [2] and [6]–[8] (W^+W^-) and [3, 4] and [9]–[11] (ZZ). Current analysis is the first one to include realistic luminosity spectra and detector simulation, which is especially important in an accurate measurement of such a subtle effect, as the phase of the amplitude.

JHEP11(2002)034

2. Vector boson production

In the narrow-width approximation the total cross section for resonant Higgs-boson production in $\gamma\gamma$ collisions, with subsequent Higgs decay into a pair of massive vector bosons VV (W^+W^- or ZZ) can be written as

$$\sigma_{\gamma\gamma\to h\to VV} = \frac{1}{\mathcal{L}_{\gamma\gamma}} \frac{d\mathcal{L}_{\gamma\gamma}^{J_z=0}}{dW_{\gamma\gamma}}\bigg|_{W_{\gamma\gamma}=M_h} \cdot \frac{4\pi^2\,\Gamma_{\gamma\gamma}}{M_h^2} \cdot BR(h\to VV)\,, \tag{2.1}$$

where the first term describes the differential $\gamma\gamma$ luminosity spectra for the projection of the angular momentum of the $\gamma\gamma$ system on the beam axis J_z, $J_z = 0$; M_h and $\Gamma_{\gamma\gamma}$ are the mass and the two-photon width of the Higgs-boson; and $BR(h\to VV)$ is its branching ratio to VV.

The Higgs-boson does not couple to $\gamma\gamma$ on the tree level. The two-photon width $\Gamma_{\gamma\gamma}$ describes the effective $\gamma\gamma h$ coupling resulting from the loop contributions of all charged particles, as shown in figure 1. In the Standard Model (SM) the dominant contribution comes from the $W^\pm$ and t loops. However, if there are any new, heavy, charged particles, they will contribute to $\Gamma_{\gamma\gamma}$ even if their mass are very high.

Presented in figure 2 (solid line) are the cross sections for the production of W^+W^- (upper plot) and ZZ (lower plot) pairs at the photon collider, expected from the Higgs-boson production and decay, as a function of the photon-photon center-of-mass energy $W_{\gamma\gamma}$. Cross sections for different Higgs-boson masses were evaluated using the HDECAY program [12] for calculating the SM Higgs-boson width and branching ratios. The total width of the Higgs resonance increases from about 0.4 GeV at $M_h = 170\,\text{GeV}$ to about 8.5 GeV at $M_h = 300\,\text{GeV}$. However, the total cross section for Higgs-boson production in photon-photon collisions slowly changes with M_h.

When studying vector-bosons production from the Higgs-boson decays, the background from direct vector-bosons production has to be considered. The non-resonant W^+W^- pair production is a tree-level process and is expected to be large. The corresponding diagrams are shown in figure 3. The cross sections for direct W^+W^- pair production for $J_z = 0$ (dashed line) and $|J_z| = 2$ (dotted line) are included in figure 2 (upper plot). The calculation was based on the scattering amplitudes presented in [6, 7].

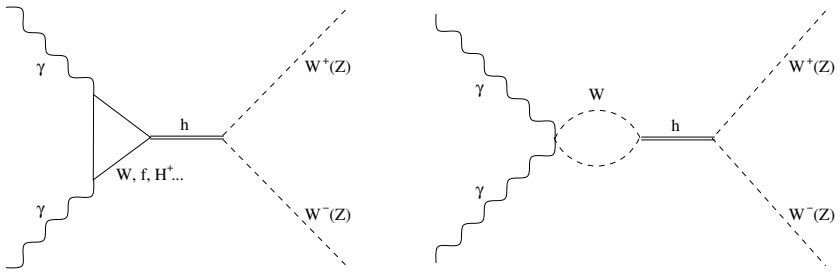

Figure 1: Diagrams for W^+W^- and ZZ pair production at the photon collider via the production and decay of Higgs-bosons.

JHEP11(2002)034

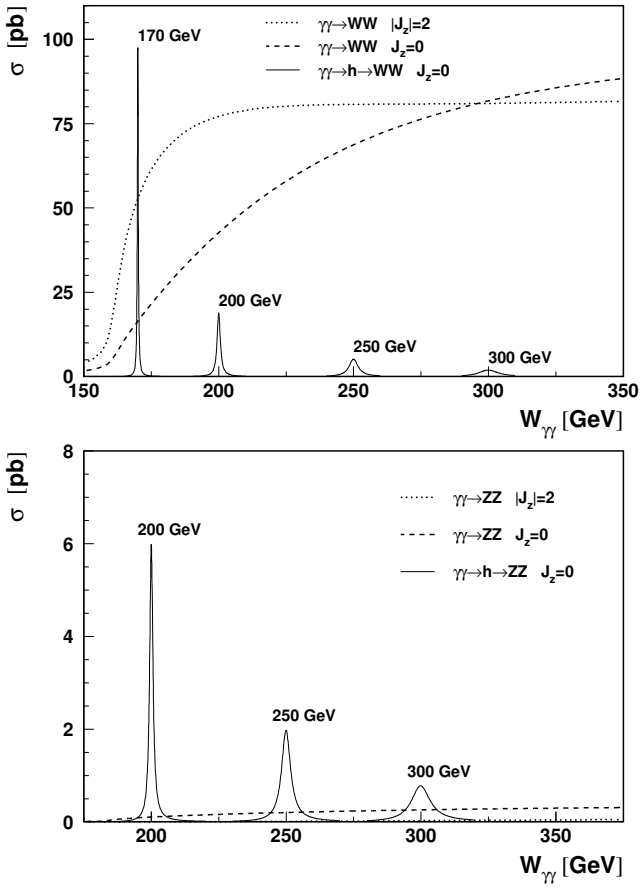

Figure 2: Cross section as a function of the photon–photon center-of-mass energy $W_{\gamma\gamma}$, for different processes contributing to the production of W^+W^- pairs (upper plot) and ZZ pairs (lower plot) at the photon collider. Cross sections for direct vector boson pair-production, for total angular momentum of colliding photons $J_z = 0$ and $|J_z| = 2$, are compared with the cross section expected from the Higgs-boson production and decay, for different Higgs-boson masses.

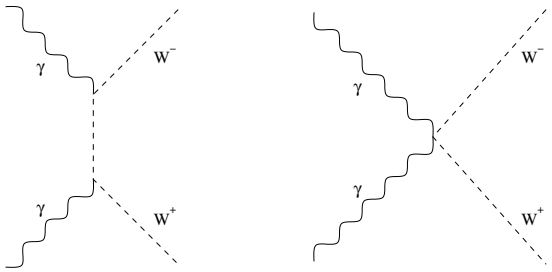

Figure 3: Diagrams for direct W^+W^- pair production at the photon collider.

For photons colliding with $|J_z| = 2$ the cross section for direct W^+W^- pair production increases fast above the production threshold and then saturates at the level of about 80 pb. The cross section for $J_z = 0$ increases slowly with the energy and reaches the same order of magnitude only at $W_{\gamma\gamma} \sim 300\,\text{GeV}$. For Higgs-boson masses above about 190 GeV, the non-resonant cross section exceeds the cross section for W^+W^- pair production from Higgs-boson decay at $W_{\gamma\gamma} = M_h$, $\gamma\gamma \to h \to W^+W^-$.

JHEP11(2002)034

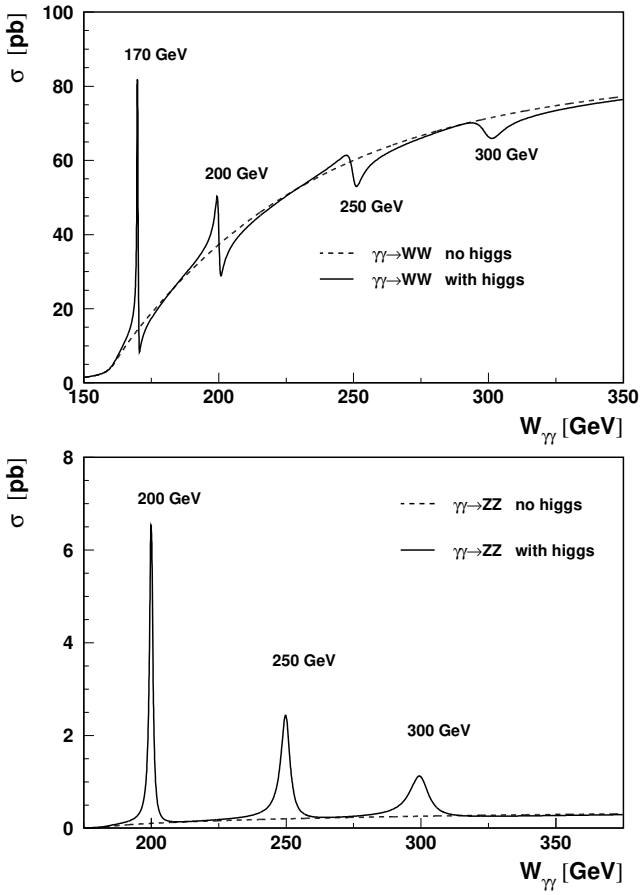

Figure 4: Total cross section as a function of the photon-photon center-of-mass energy $W_{\gamma\gamma}$, for W^+W^- pair (upper plot) and ZZ pair (lower plot) production at the photon collider, for a total angular momentum of the colliding photons of $J_z = 0$. Cross section calculated for different Higgs-boson masses, as indicated in the plots (solid line) is compared with the cross section expected from the direct vector boson pair-production (dashed line).

Direct ZZ production is only possible at the loop level. The corresponding cross sections, for $J_z = 0$ (dashed line) and $|J_z| = 2$ (dotted line), are included in figure 2 (lower plot). The cross section for $J_z = 0$ is only of the order of 100 fb. Therefore, the total cross section for ZZ pair production at $W_{\gamma\gamma} \sim M_h$ is dominated by the Higgs-boson contribution, for all considered values of the Higgs-boson mass. In the analysis presented here the asymptotic cross-section formula for $\gamma\gamma \to ZZ$ is used [3], neglecting terms of $\mathcal{O}(m_Z^2/W_{\gamma\gamma}^2)$.

For photons colliding with $J_z = 0$ the interference between the signal of vector-boson production via the Higgs resonance and the background from direct vector-boson production has to be taken into account. Shown in figure 4 are the total cross sections for W^+W^- (upper plot) and ZZ (lower plot) pair production at the photon collider, for a total angular momentum of colliding photons $J_z = 0$, as a function of the photon-photon center-of-mass energy $W_{\gamma\gamma}$. For W^+W^- pair production, very large interference effects are observed. For Higgs-boson masses above about 200 GeV, the negative contribution from the interference

JHEP11(2002)034

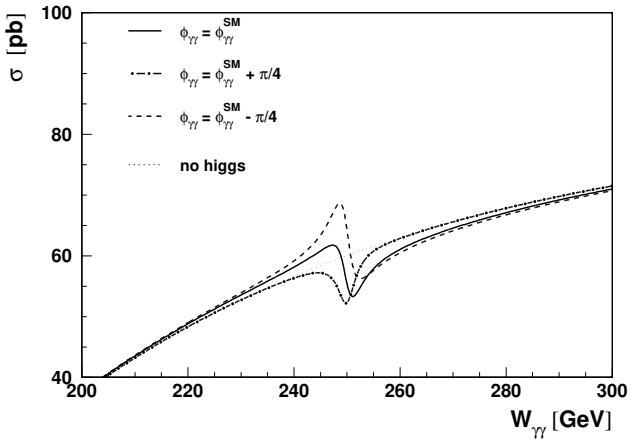

Figure 5: Total cross section as a function of the photon-photon center-of-mass energy $W_{\gamma\gamma}$, for W^+W^- pair production at the photon collider, for $M_h = 250\,\text{GeV}$ and $J_z = 0$. The cross section is calculated for an amplitude phase $\phi_{\gamma\gamma}$ equal to the Standard Model prediction $\phi_{\gamma\gamma}^{SM}$ and for a phase shifted by $\pm\pi/4$. The cross section for direct W^+W^- pair production (without Higgs-boson contribution) is included for comparison.

term is larger than the resonant (Higgs-boson only) contribution and results in the decrease of the total W^+W^- pair production cross section. For ZZ pair production the contribution of the interference term is also visible, resulting in an asymmetric Higgs resonance, but the contribution of the interference term to the total cross section is small.

The cross section for the Higgs-boson production in the $\gamma\gamma$ collisions is proportional to the two-photon Higgs-boson width $\Gamma_{\gamma\gamma}$. From the measurement of the W^+W^- and ZZ pair production cross sections at the Higgs resonance, the value of $\Gamma_{\gamma\gamma}$ can be extracted. However, the measurement of the interference term contributions allows us to access an additional piece of information about the phase of the $h \to \gamma\gamma$ amplitude, $\phi_{\gamma\gamma}$. The sensitivity of the total W^+W^- pair production cross sections to the phase $\phi_{\gamma\gamma}$ is illustrated in figure 5. Deviations of $\phi_{\gamma\gamma}$ from the value predicted by the Standard Model can significantly affect both the total W^+W^- pair production cross section and the shape of the differential cross section, although the two-photon width $\Gamma_{\gamma\gamma}$ is not changed. The measurement of $\phi_{\gamma\gamma}$ thus gives us more information about the Higgs-boson couplings, complementary to the measurement of $\Gamma_{\gamma\gamma}$.

Shown in figure 6 is the ratio of the Higgs-boson decay width $\Gamma_{\gamma\gamma}$ to the width predicted in the SM with three fermion families, $\Gamma_{\gamma\gamma}^{SM}$, as a function of the Higgs-boson mass M_h, for models with additional contribution due to one extra charged particles. The new particles considered are heavy, fourth-generation fermions (fourth-generation up quark U, down quark D or charged lepton L) or the charged Higgs-boson H^+ of the Standard Model-like Two-Higgs-Doublet Model 2HDM (II) (couplings of the lightest Higgs-boson to fermions, $W^\pm$ and Z are the same as in the SM; see also [13]). In all cases the mass of the new particle (one new particle in each model) is set to 800 GeV. For Higgs-boson masses below about 330 GeV the contribution of the new heavy charged particle to the $h \to \gamma\gamma$ vertex reduces the decay width $\Gamma_{\gamma\gamma}$, whereas for masses above about 360 GeV $\Gamma_{\gamma\gamma}$ increases in all models. For Higgs-boson masses around 350 GeV, the sensitivity of $\Gamma_{\gamma\gamma}$ to the new particles

JHEP11(2002)034

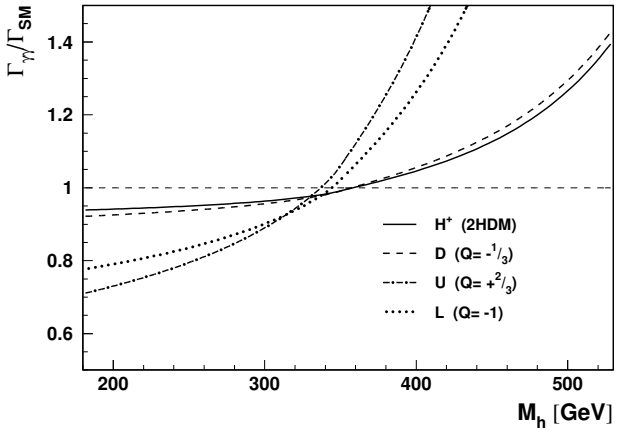

Figure 6: The ratio of the Higgs-boson decay width $\Gamma_{\gamma\gamma}$ to the width predicted in the Standard Model $\Gamma_{\gamma\gamma}^{SM}$ as a function of the Higgs-boson mass M_h, for models with additional heavy charged particles (fourth-generation d-quark D, u-quark U or lepton L, or charged Higgs-boson of the Standard Model-like 2HDM (II)).

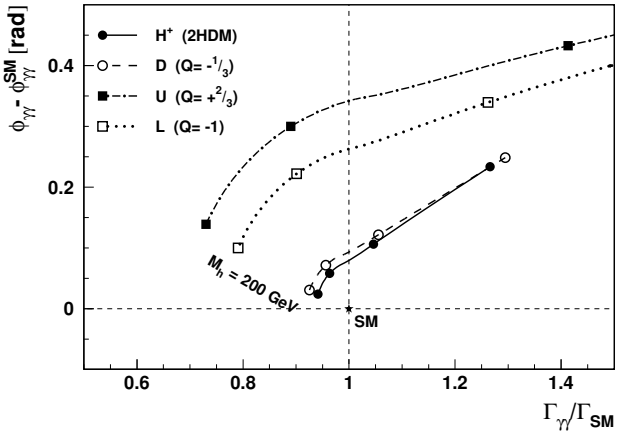

Figure 7: The difference between $\phi_{\gamma\gamma}$ and the phase predicted in the Standard Model $\phi_{\gamma\gamma}^{SM}$ as a function of the decay width ratio $\Gamma_{\gamma\gamma}/\Gamma_{\gamma\gamma}^{SM}$. Models with additional heavy charged particles (fourth-generation d-quark D, u-quark U or lepton L, or charged Higgs-boson of the Standard Model-like 2HDM (II)) with mass of 800 GeV are considered. The curves were calculated by changing the Higgs-boson mass M_h from 200 to 500 GeV; symbols are plotted every 100 GeV.

turns out to be significantly reduced, as for all considered models predicted $\Gamma_{\gamma\gamma}$ value is close to the SM expectations. However, significant deviations from the SM predictions are expected in this mass range for the phase of the $h \to \gamma\gamma$ amplitude, as shown in figure 7. If, for a Higgs-boson mass around 350 GeV, it happens that all couplings of the Higgs-boson and the $h \to \gamma\gamma$ width are the same as in the SM then the measurement of that phase is the only way to distinguish between different models.

In all cross-section calculations the electromagnetic coupling constant at the Thomson limit was used, $\alpha_{em} \approx 1/137$, as the relevant scale is the photon virtuality $Q^2 = 0$.[1]

[1] We would like to thank M. Spira and J. Kalinowski for enlightening discussions on this point.

JHEP11(2002)034

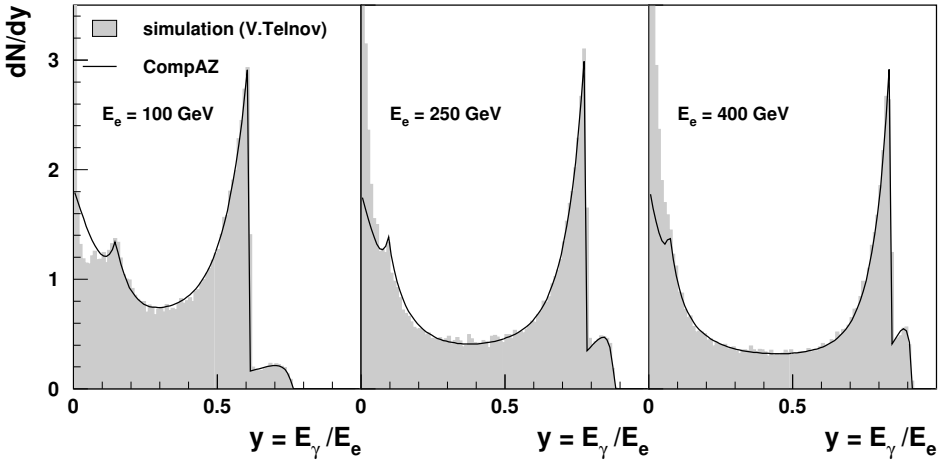

Figure 8: Comparison of the photon-energy distribution from the CompAZ parametrization with the distribution obtained from a full simulation of luminosity spectra [15, 16], for three electron-beam energies, as indicated in the plot. The cuts imposed on the energy of the second photon are 40, 150 and 260 GeV, respectively.

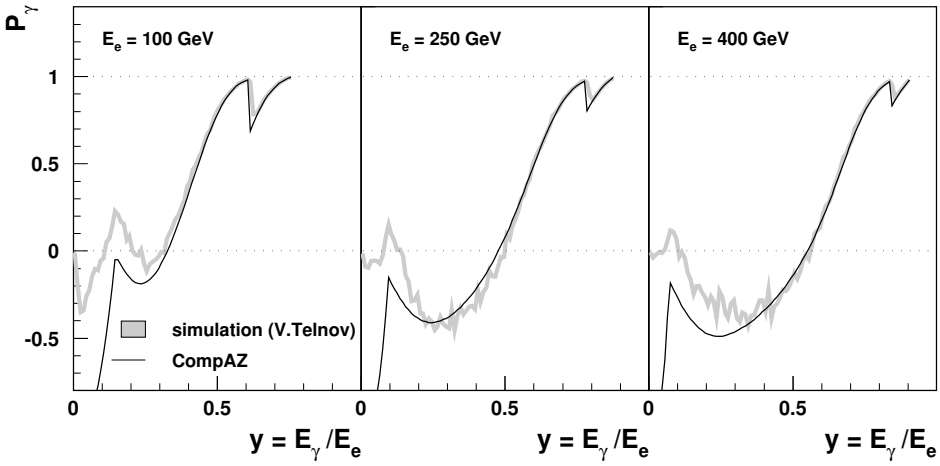

Figure 9: Comparison of the photon polarization from the CompAZ parametrization with the distribution obtained from a full simulation of luminosity spectra [15, 16], for three electron-beam energies, as indicated in the plot. The cuts imposed on the energy of the second photon are 40, 150 and 260 GeV, respectively.

3. Analysis

3.1 Luminosity spectra

In the present analysis, the CompAZ parametrization [14] of the photon collider luminosity spectra at TESLA is used. The program is based on a realistic simulation of $\gamma\gamma$ spectra [15, 16], which became available recently. Figures 8, 9 and 10 show the comparison of the photon energy, polarization and two-photon invariant mass distribution from CompAZ with the results of a full simulation. The high-energy part of the spectrum, relevant to the present analysis, is very well described.

JHEP11(2002)034

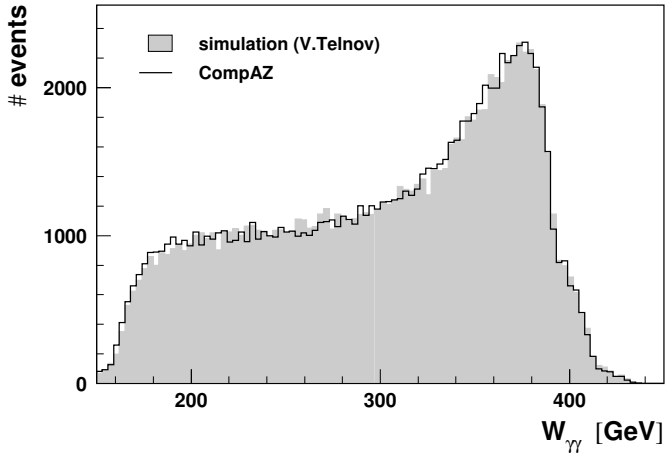

Figure 10: Distribution of the $\gamma\gamma$ center-of-mass energy for $\gamma\gamma \to W^+W^-$ events generated with PYTHIA, for an electron beam energy of 250 GeV. The sample of events generated using the CompAZ parametrization is compared with the sample generated with the luminosity spectra from a full simulation [15, 16]. The generated events were reweighted for photon polarizations.

Results presented in this paper assume one year of photon collider running at nominal luminosity. The integrated luminosity that can be obtained for $\gamma\gamma$ collisions increases from about 600 fb^{-1} for running at $\sqrt{s_{ee}} = 305$ GeV to about 1000 fb^{-1} for $\sqrt{s_{ee}} = 1$ TeV [1]. This corresponds to an integrated luminosity in the high-energy part of the spectra ($W_{\gamma\gamma} > 0.8\, W_{max}$) of 75 to 115 fb^{-1}.

3.2 Simulation

The event generation was done with PYTHIA 6.152 [17]. For $\gamma\gamma \to W^+W^-$, events generated with PYTHIA were reweighted to take into account photon polarization as well as Higgs production and interference. For $\gamma\gamma \to ZZ$, events were generated according to the cross-section formula for direct ZZ production [3] and reweighted for Higgs contribution.

The fast TESLA detector simulation program SIMDET version 3.01 [18] was used to model detector performance.

3.3 Event selection

The selection cuts were applied to select $W^+W^- \to qq\bar{q}\bar{q}$ and $ZZ \to l\bar{l}q\bar{q}$ events. The first cut is based on the requirement that four jets can be reconstructed with the Durham algorithm, with $y_{cut} \geq 0.0004$ (from the point of view of the algorithm, a jet can also be a single particle). To remove the background from semileptonic $W^{\pm}$ decays and from Z decays to neutrinos, a cut on the ratio of the total transverse momentum p_T to the total transverse energy E_T was applied. Distributions of the measured ratio p_T/E_T for $\gamma\gamma \to W^+W^-$ and $\gamma\gamma \to ZZ$ events are shown in figures 11 and 12. Neutrinoless $W^{\pm}$ and Z decays result in a narrow peak at $p_T/E_T \sim 0$. A cut $p_T/E_T < 0.1$ was applied for both W^+W^- and ZZ events.

JHEP11(2002)034

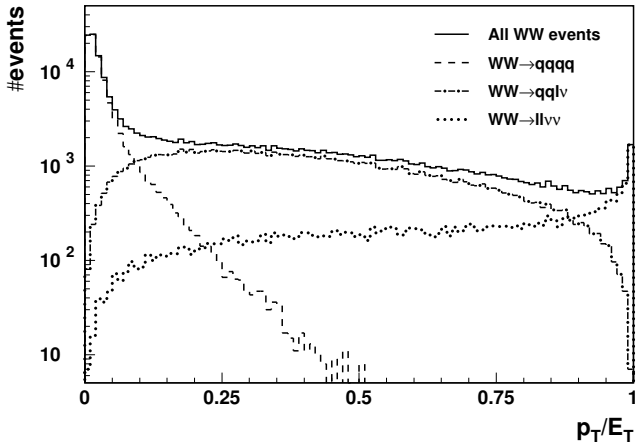

Figure 11: Measured ratio of the total transverse momentum p_T to the total transverse energy E_T for $\gamma\gamma \to W^+W^-$ events simulated with PYTHIA and SIMDET, for a primary electron-beam energy of 250 GeV. Contributions from different $W^\pm$ decay channels are indicated.

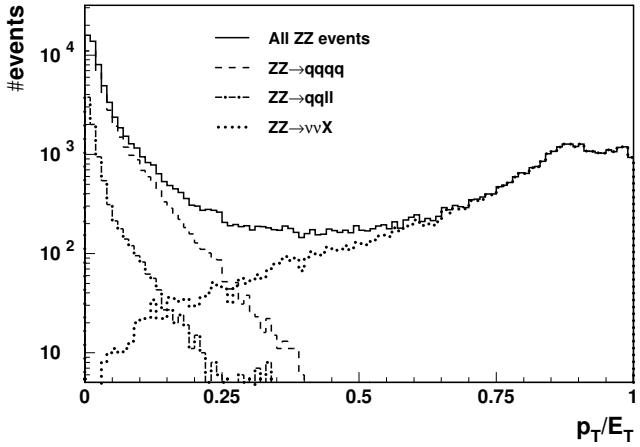

Figure 12: As in figure 11, for $\gamma\gamma \to ZZ$ events.

3.3.1 W^+W^- events

For $W^+W^- \to q\bar{q}q\bar{q}$ events, each of the four reconstructed jets should be recognized as a "true" hadronic jet. The simple algorithm used for removing jets consisting of too few particles (usually isolated leptons) requires that the number of particles in a jet be greater than 5, or that the fraction of energy carried by the most energetic particle be smaller than 95%. The next step is to reconstruct two $W^\pm$ bosons. There are three possible ways of selecting two pairs out of four jets. The configuration with the highest probability is taken, defined as

$$P_W = \prod_{W_1,W_2} \frac{M_W^2\Gamma_W^2}{\left(m_{jj}^2 - M_W^2\right)^2 + M_W^2\Gamma_W^2}.$$

The product runs over two jet pairs, m_{jj} is the jet-pair invariant mass, M_W and Γ_W are the mass and the total width of the W boson. Distribution of the probability P_W for W^+W^-

JHEP11(2002)034

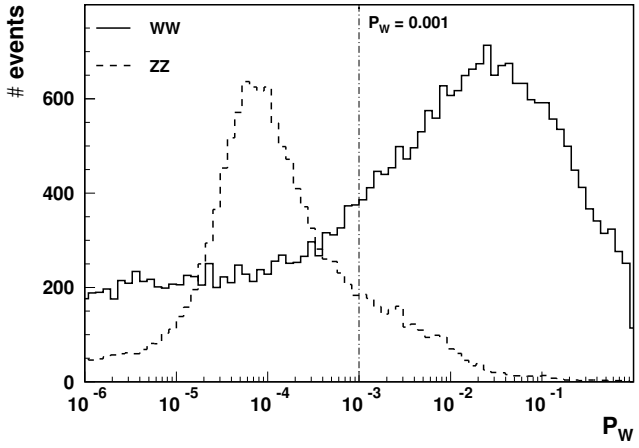

Figure 13: Distribution of the probability P_W, of four jets coming from W^+W^- pair production (for the jet configuration with the highest P_W value), for W^+W^- and ZZ events directly produced in $\gamma\gamma$ collisions, for primary electron-beam energy of 250 GeV. Only hadronic $W^\pm$ and Z decays are considered. The dash-dotted line indicates the cut used in W^+W^- event selection.

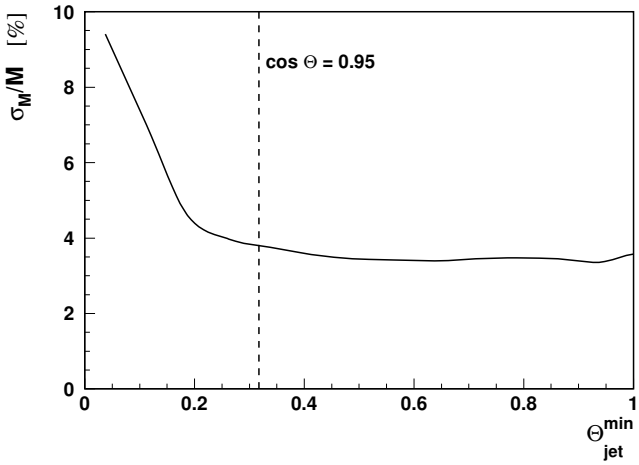

Figure 14: Relative resolution in the reconstructed four-jet invariant mass as a function of the minimum jet scattering angle θ_{jet}^{min}, for $\gamma\gamma \to W^+W^-$ events. The simulation was done using PYTHIA and SIMDET, for a primary electron-beam energy of 250 GeV. The dashed line indicates the angle corresponding to $\cos\theta = 0.95$.

and ZZ events from non-resonant production is shown in figure 13, for a primary-electron beam energy of 250 GeV. Only hadronic $W^\pm$ and Z decays are considered.

For most W^+W^- events the P_W value is above 10^{-3} whereas ZZ events result in smaller values. Separation is clear, although the mass resolution (see section 3.4) is comparable with the mass difference between $W^\pm$ and Z. For other backgrounds (e.g. $\gamma\gamma \to q\bar{q}gg$), much smaller values of P_W are expected. For the final selection of W^+W^- events, $P_W > 0.001$ was required.

For the reconstruction of $h \to W^+W^-$ events, a good mass resolution is essential. Figure 14 shows the relative resolution in the reconstructed four-jet invariant mass as a function of the minimum jet scattering angle θ_{jet}^{min}. The mass resolution deteriorates

JHEP11(2002)034

significantly if any of the jets is emitted at an angle smaller than about 0.3 with respect to the beam axis. To preserve good mass resolution, the cut on the jet angle $|\cos\theta_{jet}| < 0.95$ is imposed for all jets.

After all cuts, the efficiency for selecting $\gamma\gamma \to W^+W^-$ events is between 20% for $W_{\gamma\gamma} \sim 200\,\text{GeV}$ and 16% for $W_{\gamma\gamma} \sim 400\,\text{GeV}$.[2]

3.3.2 ZZ events

For $ZZ \to l\bar{l}q\bar{q}$ events, two out of the four reconstructed jets should be recognized as hadronic jets and the other two as isolated leptons. Only Z decays into e^+e^- and $\mu^+\mu^-$ are considered. Invariant masses of the lepton pair and of the two jets are required to be close to the Z mass. The possible background is rejected by the cut on the probability P_Z

$$P_Z = \frac{M_Z^2\Gamma_Z^2}{\left(m_{jj}^2 - M_Z^2\right)^2 + M_Z^2\Gamma_Z^2} \cdot \frac{M_Z^2\Gamma_Z^2}{\left(m_{ll}^2 - M_Z^2\right)^2 + M_Z^2\Gamma_Z^2},$$

where m_{ll} is the lepton-pair invariant mass, M_Z and Γ_Z are the mass and the total width of the Z boson. For the final selection of ZZ events $P_Z > 0.001$ was required. After all cuts, the selection efficiency for ZZ events is only about 5%, mainly due to the small branching ratio for the considered channel (9.4% for $ZZ \to l\bar{l}q\bar{q}$, $l = e, \mu$). However, the final sample is very clean. No events from the large simulated samples of W^+W^- and $f\bar{f}$ production remain after ZZ selection cuts.

3.4 Mass resolution

Figure 15 shows the error on the reconstructed $\gamma\gamma$ invariant mass for the selected $\gamma\gamma \to W^+W^-$ and $\gamma\gamma \to ZZ$ events, for $200\,\text{GeV} < W_{\gamma\gamma} < 300\,\text{GeV}$. The distributions of the

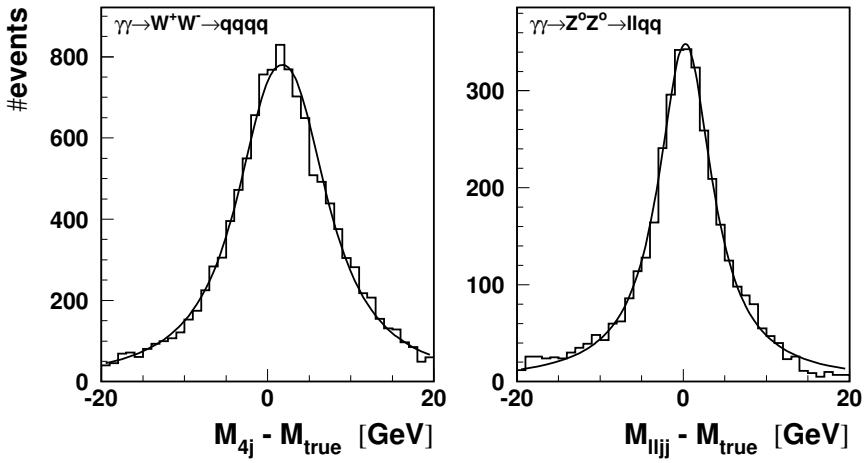

Figure 15: Resolution in the reconstructed $\gamma\gamma$ invariant mass for the selected $\gamma\gamma \to W^+W^-$ events (left plot) and $\gamma\gamma \to ZZ$ events (right plot), for $200\,\text{GeV} < W_{\gamma\gamma} < 300\,\text{GeV}$. Events were simulated with the PYTHIA and SIMDET programs, for a primary electron-beam energy of 250 GeV. The curves correspond to the parametrization used to describe mass resolution (see text for more details).

[2] The efficiencies include 47% probability for both $W^\pm$ to decay into hadrons.

JHEP11(2002)034

difference between the reconstructed and the true invariant mass, as given by the detector simulation, have a long tail. It cannot be described by a gaussian resolution; however, a good description of the detector performance is given by the modified Breit-Wigner curve:

$$P(m) \sim \frac{\Gamma^\alpha}{4(m - m_{true})^\alpha + \Gamma^\alpha} .$$

The parameters Γ and α were fitted to the simulation results in small mass bins. The value of Γ for a four-jet invariant-mass reconstruction changes from about 6.5 GeV at $W_{\gamma\gamma}$ = 200 GeV to about 13 GeV at $W_{\gamma\gamma}$ = 400 GeV. For the $l\bar{l}q\bar{q}$ final state, Γ changes from about 5.5 GeV at $W_{\gamma\gamma}$= 200 GeV to about 7.5 GeV at $W_{\gamma\gamma}$ =400 GeV. The value of α is between 2 and 2.5 for both samples.

3.5 Parametrization

The invariant-mass resolution obtained from a full simulation of W^+W^- and ZZ events based on the PYTHIA and SIMDET programs, has been parametrized as a function of the $\gamma\gamma$ centre-of-mass energy $W_{\gamma\gamma}$. By convoluting this parametrization with the CompAZ photon energy spectra and the cross sections for $\gamma\gamma \to W^+W^-$ and $\gamma\gamma \to ZZ$ processes, a detailed description of the expected mass spectra can be obtained without time-consuming event generation.

In figure 16 we show the distribution of the reconstructed invariant mass for $\gamma\gamma \to W^+W^-$ events (with an SM Higgs-boson mass of 180 GeV and an electron beam energy of 152.5 GeV) and for $\gamma\gamma \to ZZ$ events (with a SM Higgs-boson mass of 300 GeV and

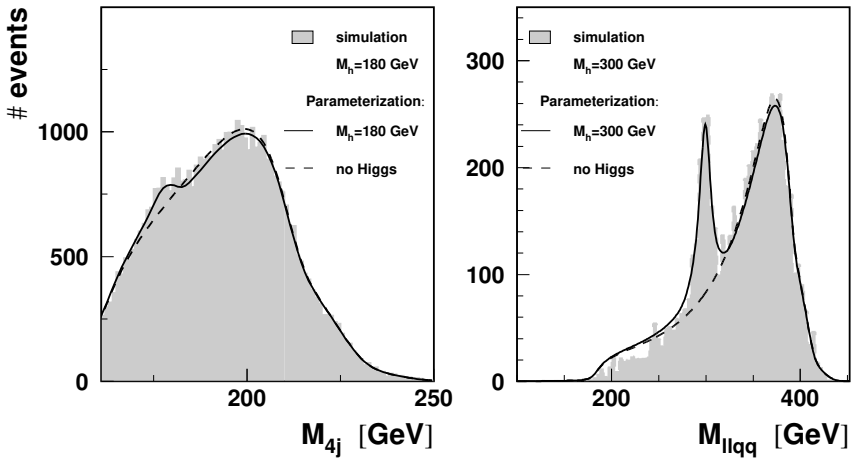

Figure 16: Distribution of the reconstructed invariant mass for $\gamma\gamma \to W^+W^-$ events with a SM Higgs-boson mass of 180 GeV and an electron-beam energy of 152.5 GeV (left plot) and for $\gamma\gamma \to ZZ$ events, with a SM Higgs-boson mass of 300 GeV and an electron-beam energy of 250 GeV (right plot). Results from the simulation based on PYTHIA and on the SIMDET detector simulation (histogram) are compared with the distribution obtained by the numerical convolution of the cross-section formula with the CompAZ photon energy spectra and parametrization of the detector resolution (solid line). The distribution expected without the Higgs contribution is also shown (dashed line).

JHEP11(2002)034

an electron beam energy of 250 GeV). Results coming from the full event simulation based on PYTHIA and SIMDET (events reweighted for the Higgs signal) are compared with the distribution obtained by the numerical convolution of the cross-section formula (including the Higgs signal) with the CompAZ spectra and detector resolution. A very good description of the measured mass distribution is obtained. Using this approach, the expected mass distributions were calculated for different Higgs-boson masses (from 170 to 390 GeV) and for different centre-of-mass energies of colliding electron beams (305, 362, 418 and 500 GeV).

4. Results

Based on the parametric description of the expected mass distributions, a number of experiments were simulated, each corresponding to one year of TESLA photon collider running at nominal luminosity, by generating Poisson-distributed numbers of observed events in bins of reconstructed mass. This was done for different Higgs-boson masses and different electron beam energies. The "theoretical" distributions were then fitted, simultaneously to the observed W^+W^- and ZZ mass spectra, with the width $\Gamma_{\gamma\gamma}$ considered the only free parameter. Figure 17 shows the average statistical error on the fitted $\Gamma_{\gamma\gamma}$ value expected after one year of photon collider running, for different masses of the Higgs-boson and different centre-of-mass energies of colliding electron beams. Standard Model Higgs-boson branching ratios are assumed. For the beam energy range considered in this analysis the two-photon width of the Higgs-boson can be measured with an accuracy of 3 to 8%, for Higgs-boson masses between 200 and 350 GeV. The precision of the measurement deteriorates with

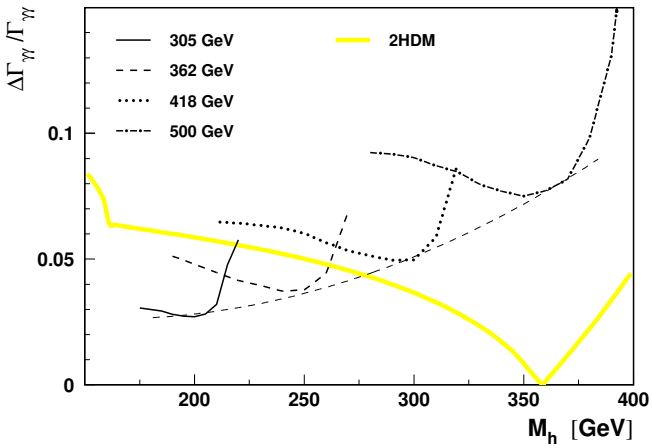

Figure 17: Average statistical error in the determination of the Higgs-boson width $\Gamma_{\gamma\gamma}$, expected after one year of photon collider running, from the simultaneous fit to the observed W^+W^- and ZZ mass spectra, as a function of the Higgs-boson mass M_h. Results are given for various centre-of-mass energies of colliding electron beams $\sqrt{s_{ee}}$, as indicated in the plot. The yellow (tick light) band shows the size of the deviation expected in the SM-like 2HDM (II) with an additional contribution due to the charged Higgs-boson of mass $M_{H^+} = 800$ GeV. The thin dashed line is included to guide the eye.

JHEP11(2002)034

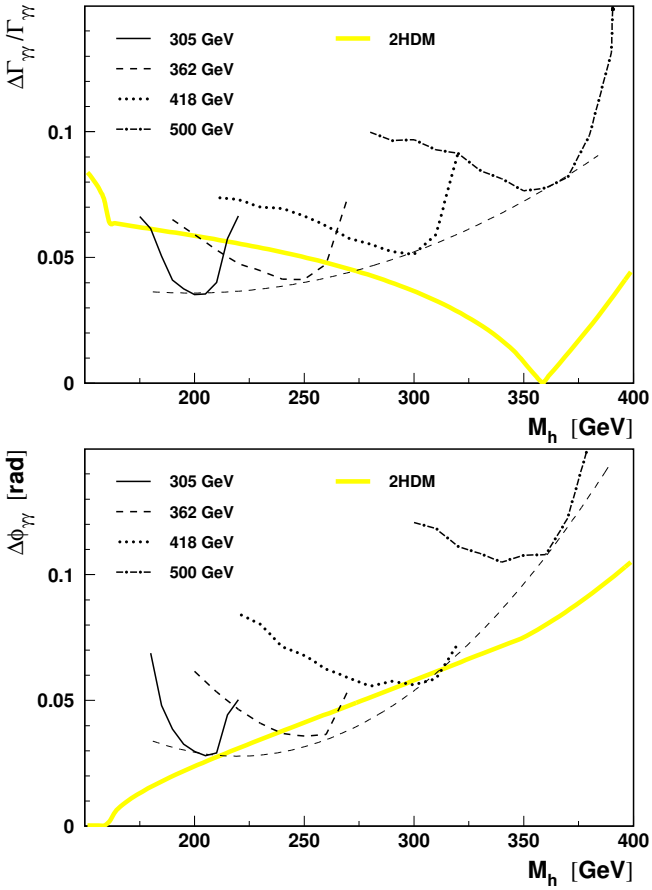

Figure 18: As in figure 17, now for a simultaneous determination of the Higgs-boson width $\Gamma_{\gamma\gamma}$ and phase $\phi_{\gamma\gamma}$ results for the width and the phase are shown in upper and lower plot, respectively.

the Higgs-boson mass. For masses above about 275 GeV the expected statistical error is larger than an effect expected in the SM-like Two Higgs Doublet Model (2HDM (II)) with charged Higgs-boson mass $M_{H^+} = 800\,\text{GeV}$.

Figure 18 shows the average statistical error expected from the *simultaneous fit* of $\Gamma_{\gamma\gamma}$ and the $h \to \gamma\gamma$ amplitude phase, $\phi_{\gamma\gamma}$ (the two-parameter fit) to the observed WW and ZZ mass spectra. The error on the extracted two-photon width of the Higgs-boson increases only slightly. On the other hand, for Higgs-boson masses between 200 and 350 GeV the phase of the amplitude can be measured with a statistical accuracy between 30 and 100 mrad. For masses between 210 and 310 GeV the expected statistical error is lower than an effect (i.e. departure from SM predictions) expected in the SM-like 2HDM (II) already after one year of photon collider running. This demonstrates that the phase measurement opens a new window to searches of processes beyond the Standard Model, in the Higgs-boson mass range where the width measurement is little sensitive to new physics.

5. Summary

Production of the Standard Model Higgs-boson at the photon collider at TESLA has been studied for the Higgs-boson masses above 150 GeV. In the considered mass range, large

JHEP11(2002)034

interference effects are expected in the W^+W^- decay channel. By reconstructing W^+W^- and ZZ final states, not only the $h \to \gamma\gamma$ partial width $\Gamma_{\gamma\gamma}$ can be measured, but also the phase of the scattering amplitude. For Higgs-boson masses around 350 GeV, the amplitude phase $\phi_{\gamma\gamma}$ is expected to be more sensitive to the loop contributions of new, heavy charged particles than the $\Gamma_{\gamma\gamma}$ itself.

The analysis presented here was based on the full event simulation, including the realistic luminosity spectra and simulation of detector effects. The parametrization of measured mass distributions was made possible by using the CompAZ spectra parametrization. Results of the fits performed for different Higgs-boson masses and at different electron beam energies indicate, that with a proper choice of the beam energy, the $\gamma\gamma$ partial width can be measured with an accuracy of 3 to 8% and the phase of the amplitude with an accuracy between 30 and 100 mrad. This opens a new window to the precise determination of the Higgs-boson couplings and therefore to searches of "new physics".

Acknowledgments

We would like to thank our colleagues from the Extended Joint ECFA/DESY Study on Physics and Detectors for a Linear Electron-Positron Collider for many useful discussions, comments and suggestions.

The work was partially sponsored by BMBF-KBN collaboration program TESLA. M.K. acknowledges partial support by Polish Committee for Scientific Research, Grant 2 P 03 B 05119 (2002), 5 P03B 121 20 (2002), and by the European Community's Human Potential Programme under contract HPRN-CT-2000-00149 Physics at Colliders. M.K. and A.F.Ż. would like to thank DESY Directoriate for kind hospitality during their stay at DESY, where part of the work was completed.

References

[1] ECFA/DESY Photon Collider Working Group, B. Badelek et al., *Tesla technical design report, part VI, chapter 1: photon collider at TESLA*, hep-ex/0108012.

[2] I.F. Ginzburg and I.P. Ivanov, *Higgs boson search at photon collider for $M_H = 140$ GeV to 190 GeV*, *Phys. Lett.* **B 408** (1997) 325 [hep-ph/9704220].

[3] G.J. Gounaris, J. Layssac, P.I. Porfyriadis and F.M. Renard, *The $\gamma\gamma \to ZZ$ process and the search for virtual SUSY effects at a $\gamma\gamma$ collider*, *Eur. Phys. J.* **C 13** (2000) 79 [hep-ph/9909243].

[4] G.J. Gounaris, P.I. Porfyriadis and F.M. Renard, *The heavy neutral Higgs signature in the $\gamma\gamma \to ZZ$ process*, *Eur. Phys. J.* **C 19** (2001) 57 [hep-ph/0010006].

[5] E. Asakawa, J.I. Kamoshita, A. Sugamoto and I. Watanabe, *Production of scalar Higgs and pseudoscalar Higgs in multi-Higgs doublet models at $\gamma\gamma$ colliders*, *Eur. Phys. J.* **C 14** (2000) 335 [hep-ph/9912373];
E. Asakawa, S.Y. Choi, K. Hagiwara and J.S. Lee, *Measuring the Higgs CP property through top quark pair production at photon linear colliders*, *Phys. Rev.* **D 62** (2000) 115005 [hep-ph/0005313].

JHEP11(2002)034

[6] G. Belanger and F. Boudjema, $\gamma\gamma \to W^+W^-$ *and* $\gamma\gamma \to ZZ$ *as tests of novel quartic couplings*, *Phys. Lett.* **B 288** (1992) 210.

[7] D.A. Morris, T.N. Truong and D. Zappala, *Higgs boson interference in* $\gamma\gamma \to W^+W^-$, *Phys. Lett.* **B 323** (1994) 421.

[8] E. Boos, V. Ilyin, D. Kovalenko, T. Ohl, A. Pukhov, M. Sachwitz and H.J. Schreiber, *Higgs search in the* WW^* *decay mode at photon linear colliders*, *Phys. Lett.* **B 427** (1998) 189 [hep-ph/9801359].

[9] G.V. Jikia, *Z boson pair production in high-energy photon-photon collisions and Higgs signal*, *Phys. Lett.* **B 298** (1993) 224; *Z boson pair production via photon fusion at a high-energy photon linear collider*, *Nucl. Phys.* **B 405** (1993) 24.

[10] M.S. Berger, *The W boson loop background to* $H \to ZZ$ *at photon-photon colliders*, *Phys. Rev.* **D 48** (1993) 5121 [hep-ph/9307259].

[11] D.A. Dicus and C. Kao, *Production of Z boson pairs at photon linear colliders*, *Phys. Rev.* **D 49** (1994) 1265 [hep-ph/9308330].

[12] A. Djouadi, J. Kalinowski and M. Spira, *Hdecay: a program for Higgs boson decays in the standard model and its supersymmetric extension*, *Comput. Phys. Commun.* **108** (1998) 56 [hep-ph/9704448].

[13] I.F. Ginzburg, M. Krawczyk and P. Osland, *Potential of photon collider in resolving SM-like scenarios*, *Nucl. Instrum. Meth.* **A472** (2001) 149 [hep-ph/0101229]; *Standard-model-like scenarios in the 2HDM and photon collider potential*, hep-ph/0101331; *Resolving SM-like scenarios via Higgs boson production at a photon collider, 1. 2HDM versus SM*, hep-ph/0101208.

[14] A.F. Żarnecki, *CompAZ: parametrization of the photon collider luminosity spectra*, hep-ex/0207021; http://info.fuw.edu.pl/~zarnecki/compaz/compaz.html.

[15] V.I. Telnov, *Principles of photon colliders*, *Nucl. Instrum. Meth.* **A355** (1995) 3.

[16] V.I. Telnov, *A Code for the simulation of luminosities and QED backgrounds at photon colliders*, talk presented at Second Workshop of ECFA-DESY study, Saint Malo, France, April 2002.

[17] T. Sjostrand, P. Eden, C. Friberg, L. Lonnblad, G. Miu, S. Mrenna and E. Norrbin, *High-energy physics event generation with Pythia 6.1*, *Comput. Phys. Commun.* **135** (2001) 238 [hep-ph/0010017].

[18] M. Pohl and H.J. Schreiber, *SIMDET - version 3: a parametric Monte Carlo for a TESLA detector*, DESY-99-030.

JHEP11(2002)034